Nuclear Inst. and Methods in Physics Research, A 980 (2020) 164444

Contents lists available at ScienceDirect

Nuclear Inst. and Methods in Physics Research, A

journal homepage: www.elsevier.com/locate/nima

Radiation damage from energetic particles at GRad-level of SiO_2 fibers of the Large Hadron Collider ATLAS Zero-Degree Calorimeter (ZDC)☆

N. Simos [a,*,1], G. Atoian [a], A. Bolotnikov [a], D. Sprouster [a,b], A. Tricoli [a], D. Medvedev [a], M. Palmer [a], D. Asner [a], N. Charitonidis [c,*], N. Mokhov [d], Z. Kotsina [e]

[a] Brookhaven National Laboratory, Upton, NY 11973, USA
[b] Department of Materials Science and Chemical Engineering, State University of New York, Stony Brook, NY, USA
[c] CERN, EN-EA, 1211 Geneva 23, Switzerland
[d] Fermi National Accelerator Laboratory, Batavia, IL 60510-5011, USA
[e] Institute of Nuclear & Radiological Sciences & Technology, Energy & Safety, N.C.S.R. "Demokritos", GR-15310 Aghia Paraskevi, Greece

ARTICLE INFO

This article is dedicated to the loving memory of our friend and colleague Nick Simos, a true pioneer of the field of radiation damage to materials and main author of this article, who suddenly passed away on 15th of July 2020. He will be dearly missed.

Keywords:
Quartz fibers
Radiation damage
Energetic protons
Fast neutrons
Transmittance

ABSTRACT

Core SiO_2 quartz fibers of the Large Hadron Collider (LHC) ATLAS Zero-degree Calorimeter (ZDC) are expected to experience integrated doses of a few giga-Rad (Grad) at their closest position to the LHC beam. An array of fibers was irradiated with 200 MeV protons and spallation-generated mixed spectra (primarily fast neutrons) at the Brookhaven National Laboratory (BNL) Linac. Specifically, 1 mm- and 2 mm-diameter quartz (GE 124) rods of 50 mm length were exposed to direct 200 MeV protons leading to peak integrated dose of ~28 Grad (~0.28 GGy). Exposure of 1 mm-diameter SiO_2 fibers to a neutron flux was also achieved in the spallation field generated by 128 MeV protons. In the post-irradiation analysis, the quartz fiber transmittance was evaluated as a function of the absorbed dose. Significant degradation of the transmittance and increased radiation damage of the material were observed. Microscopic evaluation of the fibers revealed extensive micro-structural damage and irradiation-induced defects. The measurements revealed that a threshold fluence (~2.6 10^{16} p/cm^2) or dose of ~10 Grad (0.1 GGy) appears to exist beyond which light transmittance drops below 10%. Also observed is that fiber transmittance loss increased drastically with SiO_2 fiber diameter (1 mm vs. 2 mm diameter). This is attributed, in part, to the earlier lateral leakage from the 1 mm fiber of knock-on electrons and primary protons implying that more damage-inducing protons travel within the bulk of the 50 mm long 2-mm fibers. While Monte Carlo simulations performed tend to support such assumption, future experiments and sensitivity studies are envisioned to address the fiber diameter influence on degradation.

1. Introduction

The power dissipated in the ATLAS ZDC calorimeter (Fig. 1) during the LHC p–p runs is expected to reach ~6 W/kg or ~6 kRad/s (~0.06 kGy/s) [1]. For a year of proton–proton collisions at a luminosity equal to 10^{34} cm^2/s, the expected absorbed dose will reach ~15Grad (0.15 GGy). While quartz (SiO_2) has shown resilience in high radiation environments, the GRad-level dose may have serious performance consequences in the case of radiation-induced light transmission degradation, which will affect the detector signal readout. In order to understand the properties of the SiO_2 core fibers (no cladding or coating) in the regime of such high absorbed doses, a number of irradiation experiments were carried out at 200 MeV proton Linac at Brookhaven National Laboratory.

Silicon and its oxides are the materials routinely used in various particle physics detectors and other technological applications. Some examples constitute the use of silicon in the CMS tracker of the LHC [2], the high-luminosity LHC (HL-LHC) [3] as well as space mission detectors and fusion reactor diagnostics. Specifically, for the LHC, the associated fluences for a 10-year operation are predicted to be of the order of 3×10^{15}/cm^2 and for 5 years of the HL-LHC operation -1.6×10^{16}/cm^2. In the current study, we have exposed 1 mm and 2 mm diameter SiO_2 fibers to 200 MeV direct-on protons and to a mixed spectrum of neutrons, secondary protons, electrons and gamma-rays, in two separate experiments. The doses reached in these two experiments exceed the ones anticipated in the HLLHC but perhaps not those anticipated in CERN's Future Circular Collider (FCC). Light transmittance degradation, including the damaging effect of the different

☆ Work supported by the U.S. Department of Energy.
* Corresponding authors.
E-mail address: nikolaos.charitonidis@cern.ch (N. Charitonidis).
[1] Deceased.

https://doi.org/10.1016/j.nima.2020.164444
Received 29 February 2020; Received in revised form 14 July 2020; Accepted 16 July 2020
Available online 18 July 2020

particles (protons vs. neutrons) on SiO_2 fibers, and radiation-induced fiber micro-structural damage were observed & studied.

Prompted by the potential applications in particle accelerator detectors and reactor environments, a fairly large body of research has been generated to-date. Silicon sensors for the Compact Muon Solenoid (CMS) detector of LHC were electrically qualified [2] following irradiation with 26-MeV protons and neutrons. The sensor leakage current, along with the full depletion voltage under irradiation and long-term reverse annealing were assessed. Differences between neutron and proton irradiation on depletion voltage have been observed. Correlation between radiation-induced defects, and the optical properties of pure fused silica-core optical fiber, under gamma-ray irradiation in air at 1273 K was reported in [3]. Using high resolution-transmission electron microscopy (HR-TEM), Tsuchiya and coworkers showed that radiation-induced crystallization of SiO_2, ~10 nm in diameter, formed in the irradiated optical fiber, has important influence on the optical transmission and luminescence properties. In [4], the point defects induced in radiation hard optical fibers were investigated using both mixed source of neutrons (fluences from 10^{15} to 10^{17} n/cm^2) and γ -rays (doses from 0.02 to 2 MGy) as well as by a sole γ -ray source (dose up to 10 MGy). Similarities in spectroscopic properties of the induced defects were identified in two irradiations for up to 10^{16} n/cm^2 when the correlation broke down and growth of a photoluminescence was observed at around 10^{17} n/cm^2. E. Colby, et al. [5] obtained transmission spectra for a broad array of materials that include differing thicknesses of quartz, Si, a-SiO_2, c-SiO_2 using a ^{60}Co γ-source, where the transmittance dependence on the absorbed radiation dose was shown.

M. Jaksic, et al. [6] compared results of proton irradiation with irradiation from ^{60}Co γ-source on a series of FZ PIN diodes. In [7] structural damage, defect formation and phase transitions in fused silica irradiated by fast neutrons over a broad fluence range (10^{17}–10^{21} cm^{-2}) was studied using reflectance spectroscopy, X-ray scattering, and luminescence spectroscopy. Dose dependence was determined for spectroscopic, diffractometric, and luminescent properties. Specifically, the mechanism of defect formation in fused silica was studied revealing that low-energy ionization processes generate defects in the fused silica while the rate of defect formation is strongly dependent on irradiation temperature. Optical fibers with silica core were examined during irradiation in a fission reactor [7]. According to [7] the fibers showed radiation resistance, especially at higher temperatures, and for wavelengths longer than 0.7 μm up to the fast neutron fluence of 1.06×10^{20} n/cm^2 and the gamma ray dose rate of 4.3 10^9 Gy at 460 K. Optical emissions induced by the reactor irradiation were observed during irradiation. The optical transmissivity in fibers was measured in situ [8] during fast neutron and gamma irradiation, up to doses of 2 10^{24} n/m^2 and 5×10^9 Gy, respectively at irradiation temperature ranging from 300 to 700 K. It was shown in [8] that the effects from irradiation with fast neutrons were different from those ionizing irradiation only. Important to note is that some fibers were found to withstand the heavy irradiation, especially in an infrared wavelength range. The optical and dosimetric characteristics of fused silica quartz (pure silica quartz core, no cladding) was studied in [9] under γ-rays, reactor neutrons and protons. Optical density change at 550 nm was used as matric to evaluate the different grades. Important finding [9] that is extremely relevant to the present work is that saturation of the optical density at 550 nm was observed at ~10^{16}n/cm^2 and at ~10^{14}p/cm^2. Furthermore, it was shown in [9] that the optical density evolution with absorbed dose exhibited kinks under γ-rays and neutrons. Such behavior was explained in [9] as likely the process being dominated by existing defects in the quartz fiber structure over the lower absorbed dose regime and by defects induced by radiation over the higher absorbed dose regime.

The behavior of special sensors/detectors in adverse radiation conditions such as those found in space or nuclear facilities is also of great interest. For example, in nuclear environments optical fibers occupy a niche in optical communication links, embedded into various all-fiber or hybrid sensors or as light-guides for control and diagnostics [10–19]. In a more recent review study [20] the main defects responsible for the fiber degradation when exposed to transient irradiations (fusion facilities) or steady state ones (fission, high energy physics facilities) in the 300 nm–2000 nm spectral domain were discussed. Macroscopic effects such as radiation induced attenuation, emission and the radiation-refractive index change were addressed. In [20] the degradation attributed mainly to the generation of point defects in the amorphous glass (SiO_2) of the fiber's core and cladding layers by ionization or displacement damage caused by radiation. Radiation-tolerant sensors for pixel detectors motivated by the HL-LHC are discussed in [21]

In this work we report the results of transmittance measurements of 1 mm and 2 mm diameter SiO_2 core fibers – fiber refers in this study to the pure quartz core with no cladding or coating – after the irradiation with 200 MeV protons and 1 mm diameter fibers after irradiation with spallation, secondary particles dominated by fast neutrons. In both cases the specimens accumulated the dose of 0.48 GGy. Further, close examination of irradiated fibers was conducted under optical microscope to assess the structural changes from the interaction with the high-energy particles. Results of extensive Monte Carlo simulations of the experiments, including analyses carried out to address the effect of the fiber diameter and thus the performance degradation were also reported.

2. Experimental

2.1. SiO_2 quartz fiber irradiation

The Brookhaven proton Linac and the Linac Isotope Production beamline/end station (BLIP) [22] were used for the two SiO_2 fiber irradiation experiments. The first of the two experiments, used the primary 200 MeV protons and the second experiment utilized the spallation-generated radiation field that consisted primarily of fast neutrons and gamma rays of a very broad energy range and which was generated from spallation of 118 MeV protons on an array of medical isotope targets. This radiation environment, closely resembles the one existing in the ATLAS cavern. During phase I of the study, the beam of 200 MeV protons was directed to an array of 1 mm and 2 mm diameter SiO_2 fibers as shown in Fig. 2b for a total accumulated charge of 72.24 μAh. The proton beam position, determined with a plastic foil before irradiation, is superimposed on the positions of the three fiber capsules made of aluminum (Fig. 2a). Based on this measured beam position, the fluences and corresponding dose values received by the three capsules/canisters were calculated using MARS & FLUKA [23–25] Monte Carlo codes, taking into account the beam position information, and its Gaussian distribution profile (σ_1, σ_2 and beam offset shown on Fig, 2b). The fluences were estimated to be 2.5 10^{15} p/cm^2, 7.3 10^{16} p/cm^2 and 2.6 10^{16} p/cm^2. Previous studies [9], where various grades of fused silica were irradiated with 20 MeV protons, and mixed reactor irradiation (neutrons and γ-rays) showed similar dependence of the optical density with the absorbed energy when comparing the two irradiations and at the same time revealing that saturation can be reached with proton fluence an order of magnitude lower. While the anticipated dose at the ATLAS ZDC is primarily from neutrons and γ-rays, the similar behavior observed under protons led-us to pursue irradiations with direct, 200 MeV protons, them being a good tool for assesing the radiation damage of the fibers.

After the irradiation, the residual activity of each individual fiber was measured and, based on its position with respect to the beam footprint, the corresponding dose was estimated. Fibers within one σ (capsule 2) of the beam received a dose of ~28 Grad (~0.28 GGy) while fibers in the other two positions (or capsules) received 10 and 5 Grad (0.1 and 0.05 GGy) respectively.

Fig. 3 shows the estimated energy deposited by the proton beam during the 200 MeV irradiation. Fig. 3a depicts the energy deposition

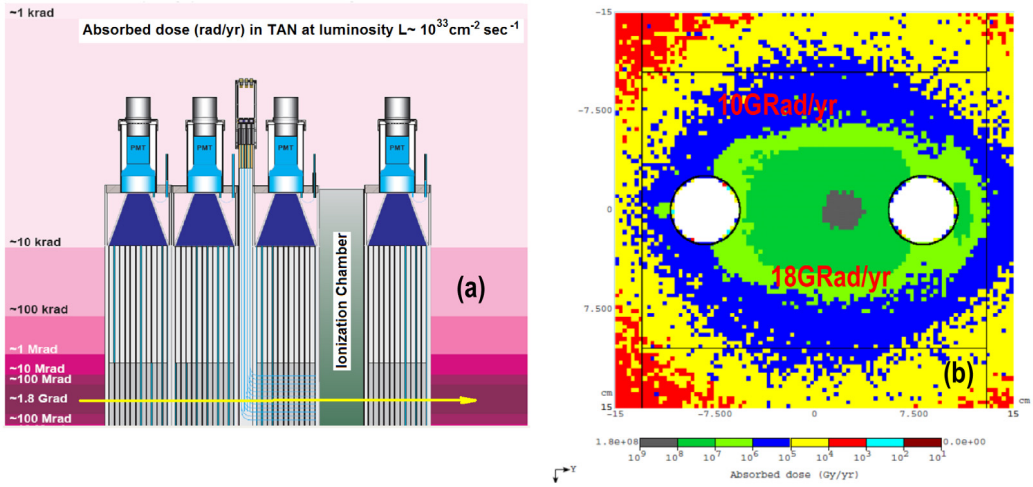

Fig. 1. (a) Configuration of ZDC Calorimeter in LHC depicting the anticipated dose levels and (b) isocontours of hadron flux (cm^{-2} s^{-1}) and yearly accumulated dose ZDC in SiO_2 fibers.
Source: From Ref. [1].

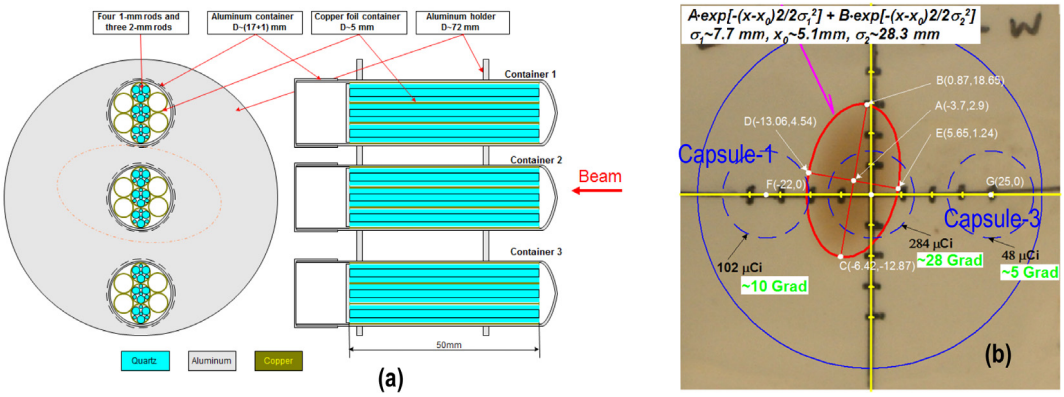

Fig. 2. (a) Schematics of 1 mm and 2 mm quartz (GE 124) fiber arrangement enclosed in 0.5 mm thick aluminum container for the 200-MeV proton irradiation, (b) dose to the capsules, calculated based on the measured position and shape of the 200 MeV incident proton beam.

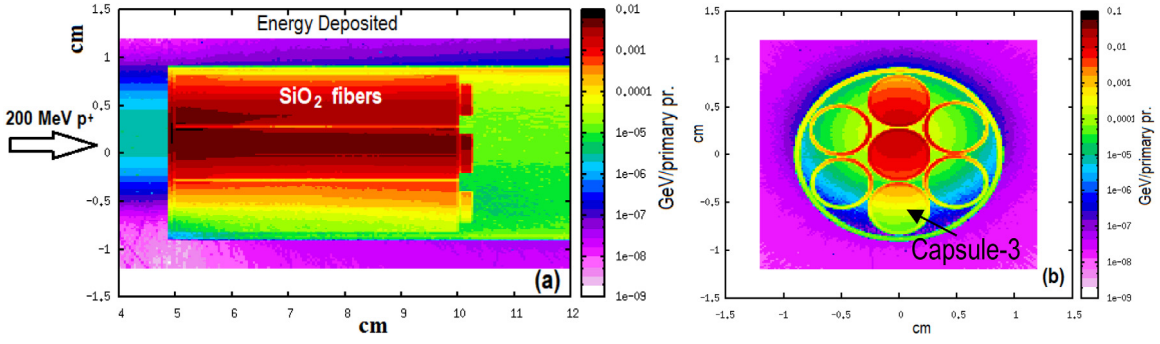

Fig. 3. FLUKA geometry model used for the simulations. (a) Energy deposited along the SiO_2 fibers, (b) cross sectional profile of deposited energy. (Note that only the middle raw of three capsules contain the fibers, the pairs of capsules on either side were used for the proper positioning of the assembly.)

in a cross section parallel to the long dimension of the fibers (50 mm long) and Fig. 3b over a cross section normal to the fiber long direction (note that Fig. 3b has been rotated 90° counter-clockwise, relative to the foil beam footprint shown in Fig. 2b). The four circles (two on either side) of the three capsules shown in Fig. 3b depict the empty capsules used in the experiment for securing the positions of the three middle capsules containing SiO_2 fibers. Fig. 4 depicts the experimental set up during the second experiment (mixed spectra irradiation) as well as the spallation-generated neutron and gamma ray profiles by the 118 MeV protons. Shown in Fig. 5a is a schematic of the three fiber capsules superimposed with the proton beam Gaussian shape and estimated dose values. Fig. 5b shows measured fiber activity in the three capsules of the 200 MeV proton irradiation.

In the second experiment, spallation neutrons generated from 118 MeV protons impinging and stopped by an array of targets located upstream of the SiO_2 capsules were utilized. The resulting mixed field irradiating the fibers this time, consisted primarily of fast neutrons (>0.1 MeV) and gammas (see Fig. 4). For this irradiation, only two capsules containing 1 mm diameter SiO_2 fibers were used. Fig. 6 depicts the energy spectra of the spallation neutrons and gamma rays in the

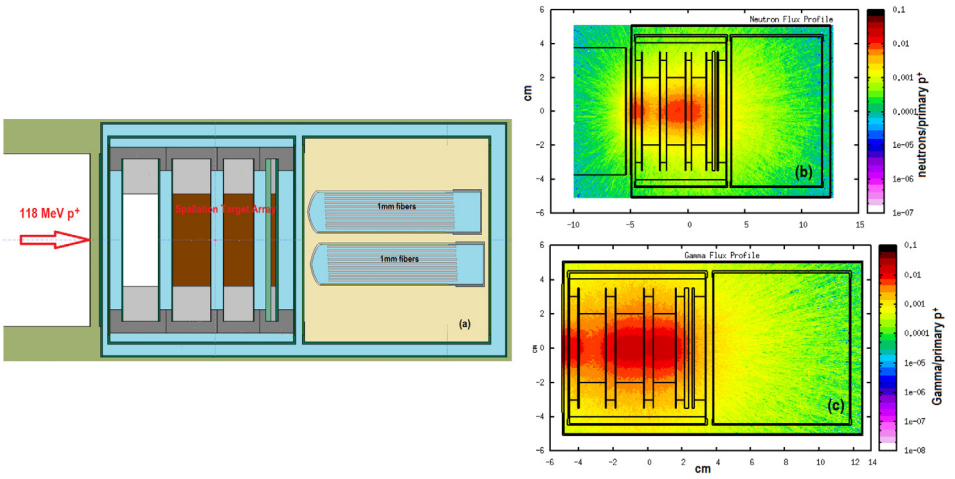

Fig. 4. Schematics of the experimental set-up for 1 mm diameter SiO_2 fibers irradiated in the mixed field of fast neutrons and gammas. (a) cross sectional view of the experimental set up, (b) map of generated neutron flux, (c) map of generated gamma ray flux.

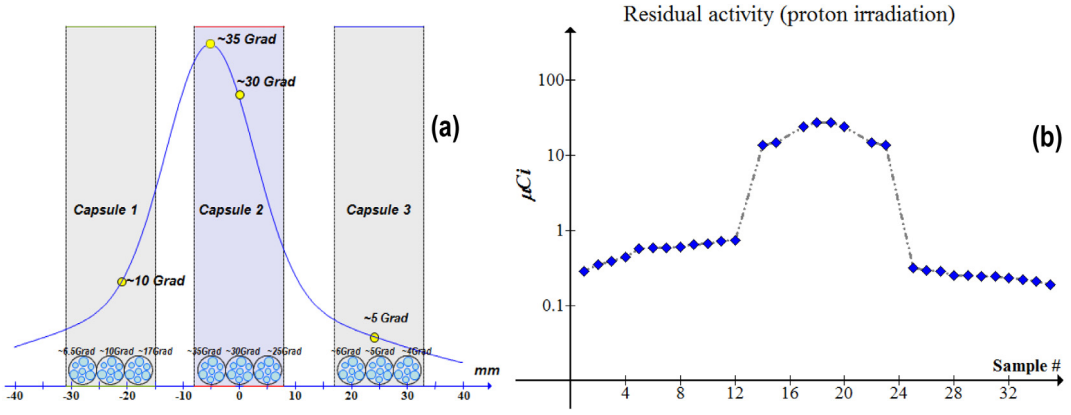

Fig. 5. (a) Beam profile with estimated dose, (b) measured total residual activity of SiO_2 fibers.

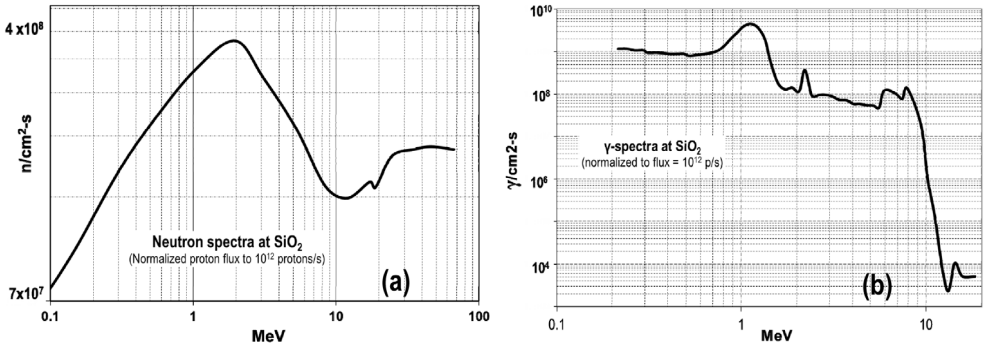

Fig. 6. Simulated (a) neutron and (b) γ energy spectra at the SiO_2 array of the second irradiation experiment (Fig. 4) of 1 mm diameter fibers.

location of the SiO_2 fibers [23]. In this case, 23,964 μA-h of 118-MeV protons were stopped in the isotope targets upstream (see Fig. 4) predicted to reach comparable dose levels to those of first (200 MeV primary proton) experiment.

Measurements of residual activity (μCi) were performed both for each fiber individually and for each of the irradiated assemblies of samples after the end of bombardment. This was done (a) to provide an assurance that both irradiation phases delivered substantial integrated dose, and (b) to assess the variation in the absorbed dose from sample to sample within each capsule (Fig. 7). This in turn, allows the estimation of the effects of the dose (or activity per fiber) on the transmittance degradation. The latter is discussed in the next section (Figs. 10a and 10b).

3. Post-irradiation analysis of siO_2 fibers

3.1. Photon spectra

Fig. 8 depicts the photon spectra collected from neutron-irradiated fibers using a high purity Ge detector (HPGe) showing the 511 keV annihilation peak and the dominant gamma-ray peak at ~1274 keV corresponding to Na-22.

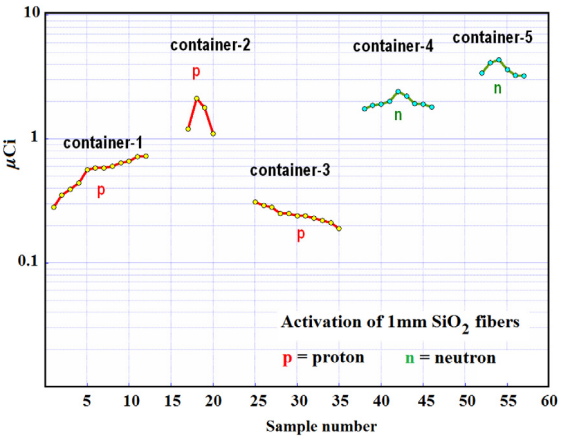

Fig. 7. Residual activity (μCi) in proton and fast neutron irradiated 1 mm diameter SiO_2 fibers.

3.2. Transmittance measurement

The degradation of the light transmittance in the fused silica fibers as a result of exposure to the two types of radiation (200 MeV protons and spallation neutrons) was evaluated using the set-up shown in Fig. 9. The experimental set up was built at Brookhaven National Laboratory. Three light wavelengths (violet $\lambda = 405$ nm, blue $\lambda = 470$ nm and red $\lambda = 630$ nm) were transmitted via LED in pulsed (flash) mode to estimate the transmittance $T(\lambda)$ based on transmitted power $I(\lambda)$ and incident power $I_0(\lambda)$[$T(\lambda) = I(\lambda)/Io(\lambda)$].

Fig. 10 summarize the post-irradiation transmittances exhibited by the irradiated fibers. Specifically, the transmittance is plotted against the corresponding residual activity on the same graph for correlation. It is noteworthy, that fibers exposed to 200-MeV protons and located within the beam σ (dose of ~28 GRad) have completely lost all their transmittance properties. The same is true for all the 1 mm fibers that were exposed to the spallation neutron flux as described above and were located where the flux was approximately uniform. Transmittance in this case, as in the 28 Grad (0.28 GGy) proton irradiation, was diminished (as indicated in Fig. 10). The apparent trend in the data of Fig. 10a, depicting the 1 mm fiber measurements from the same capsule, stems from the variation of damage due to the different positioning of each fiber in the bundle with respect to the impinging beam.

The correlation of the absorbed dose and the light wavelength transmittance for doses up to 15 Grad (0.15 GGy) is depicted in Fig. 11. The transmittance degrades substantially with dose elevation up to 8 Grad. From 8 to 15 Grad the transmittance stays at approximately 10%. Based on the results of both irradiation experiments, it can be concluded that a dose of ~8 Grad (0.08 GGy) represents a threshold beyond which light transmission property degrades substantially in Silicon-based materials. In ref. [9] the presence of "kinks" (or steps) in the relation between optical density and absorbed dose were observed and discussed. These changes were attributed to the dominance of pre-existing defects in the fibers during the low dose (lower effect) and to the effects of radiation-induced damage in the microstructure in the higher dose (higher effect). The similar effect or process could explain the distinct step (or "kink") observed in the transmittance in this study shown in Fig. 11.

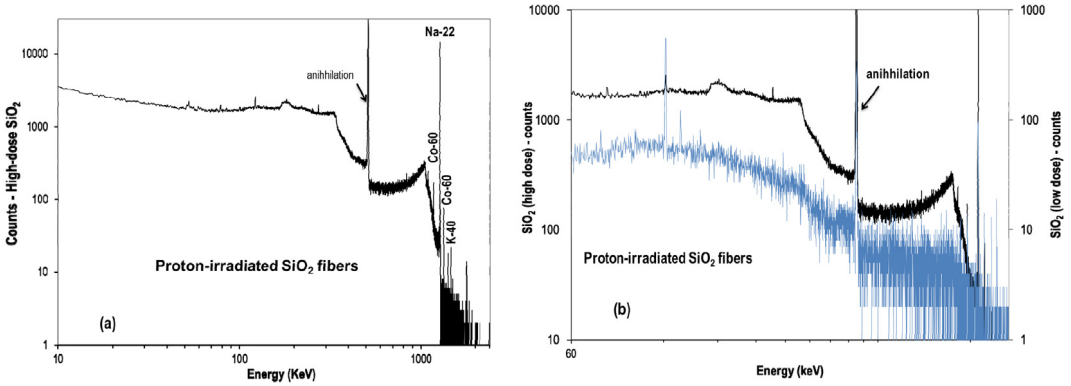

Fig. 8. (a) Photon spectra of proton-irradiated SiO_2 fiber, (b) close up of the low-energy regime.

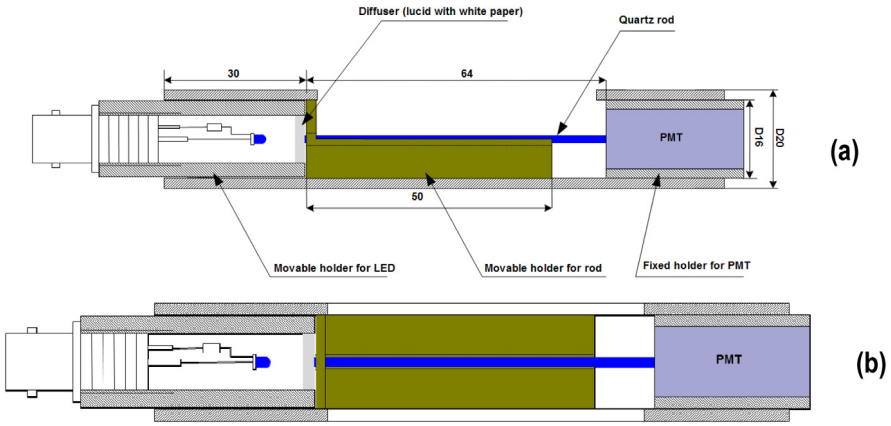

Fig. 9. Cross sectional view (a) and plan view (b) of SiO_2 fiber transmittance measurement set-up.. (For interpretation of the references to color in this figure legend, the reader is referred to the web version of this article.)

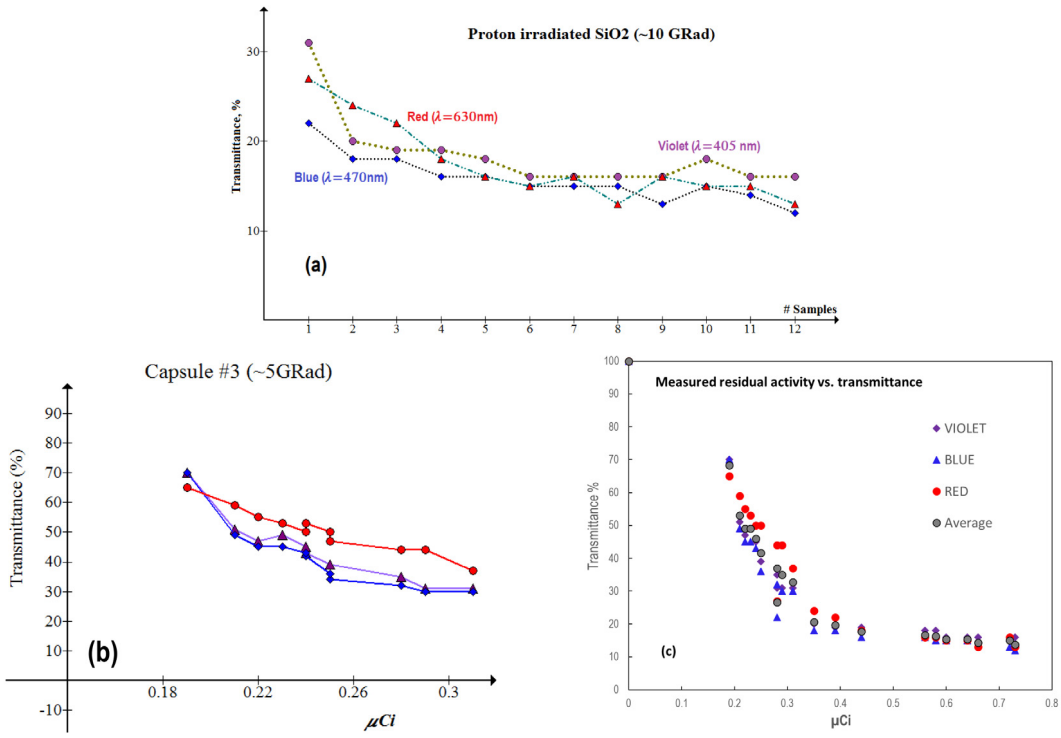

Fig. 10. (a) Variation of the measured transmittance for the 1 mm fiber in the array estimated to have received 10 Grad dose (sample number simply denotes measured fiber from the bundle), (b) variation of transmittance for all three wavelengths in 1 mm fibers of capsule #3 estimated to have received 5 Grad dose as a function of measured residual activity of each fiber, (c) transmittance vs. measured residual activity of 1 mm fibers in all three capsules. The color in the traces (violet, blue and red) correspond to different light wavelengths λ, equal to 405 nm, 470 nm and 630 nm respectively.. (For interpretation of the references to color in this figure legend, the reader is referred to the web version of this article.)

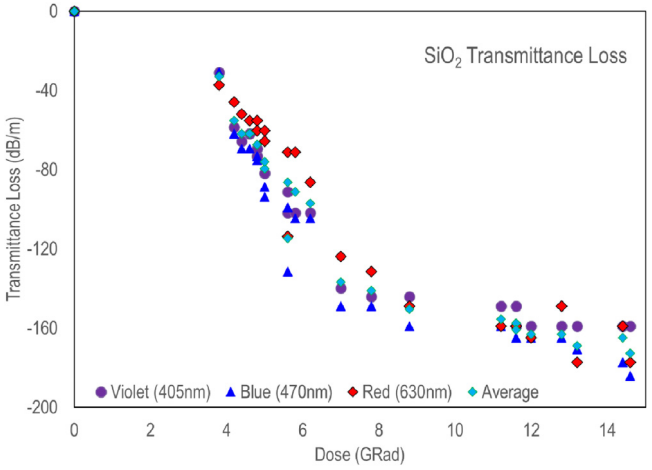

Fig. 11. Light wavelength transmittance loss (dB/m) vs. calculated dose.

3.3. Size dependent performance in 1 mm and 2 mm diameter fibers

The transmittances of the 2 mm diameter SiO_2 fibers for blue (470 nm) and red (630 nm) wavelengths and for the bundles (capsules) that received 5 Grad and 10 Grad dose was compared to that of their 1 mm-diameter counterparts (Fig. 12). For the 2 mm-diameter fibers, the transmittance of blue (470 nm) and red (630 nm) wavelengths only were measured. The measurements revealed the loss of transmittance in the 2 mm-diameter fibers to be much greater than their 1 mm-diameter counterparts. The remaining transmittance in the 2 mm diameter fibers (on average) is approximate 5x lower than the corresponding remaining transmittance in 1 mm fibers (Fig. 12).

To provide further insights into the reasons for the observed dramatically different response of the 1 mm and 2 mm fibers, the interaction of 200 MeV protons with 50 mm long SiO_2 fibers (1 mm and 2 mm diameter) was modeled in FLUKA Monte Carlo code [24,25]. For the simulation, production of knock-on electrons (down to a keV region with their production at large angles) as well as the large angle Coulomb scattering of beam protons themselves (in addition to multiple Coulomb scattering) were implemented. Fig. 13 shows the simulated proton beam profiles for the 1 mm and 2 mm diameter fibers. Particularly, the 200 MeV proton beam impinged onto the upstream face of the 50 mm long fiber, along its longer direction, similar to the actual irradiation experiment. The proton beam, with a simulated Gaussian shape for each case (1 mm vs. 2 mm) was adjusted such that 50% of the incoming beam protons impinged (entered) the upstream face of each fiber in both cases. In other words, for the type of analysis performed, this implied the same number of protons interacting with each fiber. A second scoring detector with the same cross-sectional area as the fiber was positioned at the downstream face to record the percentage of the beam that has made it up to that point. A different option/analysis (not exercised herein) would have been the consideration of relevant fluences between detectors placed on the upstream and downstream faces of each fiber. The adopted beam-fiber interaction model shown in Fig. 13 has shown that a smaller percentage of the primary beam entering the cross section of the 1 mm diameter fiber actually leaves the fiber from the downstream face that in the case of its 2 mm diameter counterpart. It is only the authors' assessment, and until further experimental exploration backed by sensitivity analyses over several parameters including fluence uniformity over the two fiber cross sections, incidence angle, fiber cross-communication (i.e. leaked protons from thinner fiber interacting with neighboring fibers), etc., that the observed higher deterioration of transmittance in the 2 mm diameter fibers at least partly stems from the higher leakage of beam protons leaving the 1 mm fiber. This is believed to be driven by the interaction lateral leakage of knock-on electrons from the 1-mm fiber compared to the 2-mm one as

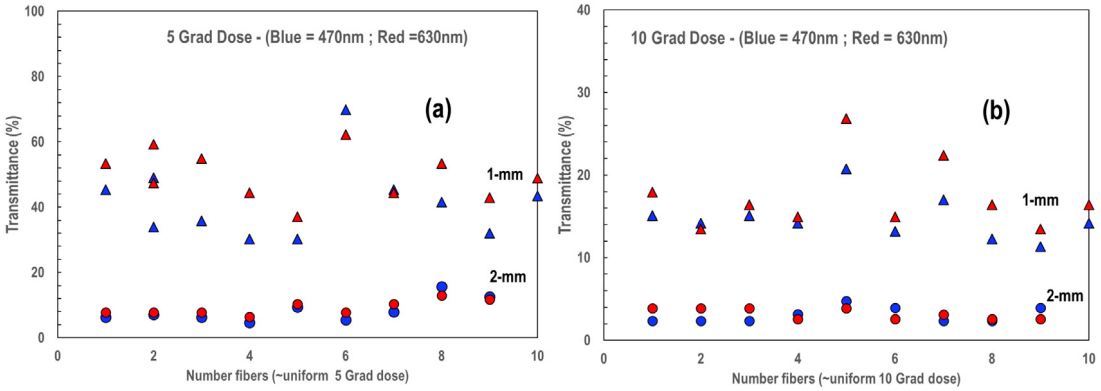

Fig. 12. Comparison of two different wavelength transmittance vs. calculated dose in 1 and 2 mm fibers. (a) at 5-Grad dose, (b) 10-Grad dose.. (For interpretation of the references to color in this figure legend, the reader is referred to the web version of this article.)

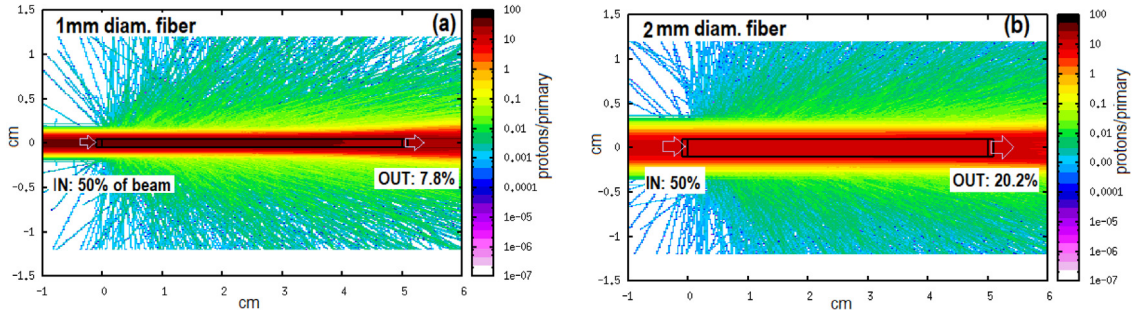

Fig. 13. Schematic representation of the interaction of the proton beam with 50 mm long SiO_2 fiber with. showing lateral leakage of primary protons. (a) 1 mm diameter, (b) 2 mm diameter.

primary protons travel along the fiber. In other words, more incident protons remain and interact within the bulk and along the length of the 2 mm fiber which likely to also be bombarded with protons leaking out of neighboring 1 mm fiber accumulating more the damage along the thicker fiber's length. In future work, the convoluted relationship between impinging primary particle angle relative to fiber orientation and fiber diameter will be explored both experimentally and through Monte Carlo based simulations considering the cross-fiber interaction accompanied by fine characterization of the induced microstructural damage along the length of fibers with different diameters.

3.4. Microscopic assessment of damage

The interaction of the energetic particles with the crystal atoms and the structural disorder that results from it, is the reason for the observed loss of transmission. Features that constitute damage can be seen in crystals on a TEM image. Filaments of atomic disorder or fragment tracks have been observed in non-metals as well as thermal spikes resulting in localized material phase transformation. In ref. [3] it was shown that the amount of polycrystalline material increases with radiation (following post-irradiation annealing) while no polycrystalline material is detected for annealing to similar temperatures in unirradiated materials. It was therefore assessed that the production of SiO_2 crystals significantly influences the optical transmission and luminescence properties.

Using a Keyence VHX-1000 Digital microscope (10k × magnification) which, in addition to the surface features, following the fiber interaction with neutrons or protons, enables illumination from bottom to generate a composite mesh that provides a view within the bulk (subsurface), 1 mm fibers were examined. Figs. 14a and 14b and 14c depict surface features of unirradiated and neutron-irradiated 1 mm diameter fibers. Fig. 14c is depicting the state of the fiber within its bulk revealing extensive crystal defect that have developed following

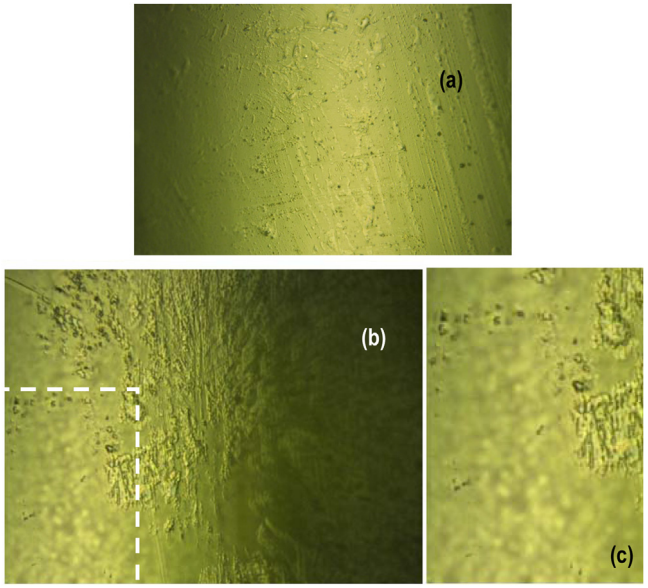

Fig. 14. (a) Unirradiated 1 mm-diameter SiO_2 crystal surface, (b, c) following spallation (primarily fast neutron and γ-irradiation). The width of the left image is 500 μm.

irradiation with energetic particles (several GRad dose). This crystallization network of the SiO_2 is believed to have dramatically influenced the optical transmission degradation (~100% reduction)

Fig. 15 depicts damage features at the surface of the fiber confirming the presence of fragment tracks and "thermal spikes".

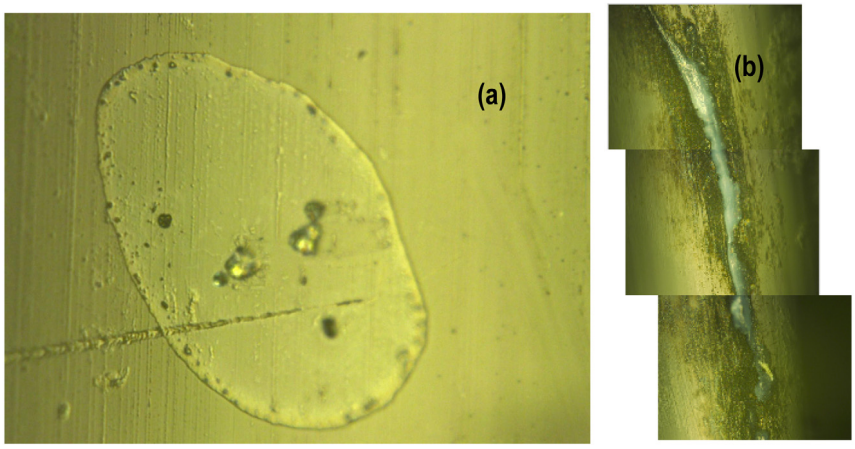

Fig. 15. (a) Thermal spike on the SiO_2 fiber surface and (b) observed fragment track (image width 500 μm).

4. Summary

The SiO_2 quartz fibers of the Zero-degree Calorimeter (ZDC) in the LHC ATLAS receive integrated doses of a few GGy. The experimental effort focusing on radiation damage on SiO_2 crystal fibers of the LHC ZDC detector showed that Grad-level irradiation has a detrimental effect on the fiber light transmittance. Microscopic analysis has revealed that lattice disorder induced by irradiating particles such as protons and or neutrons is the most likely cause of the observed light transmittance degradation.

The study established a very crucial threshold of fluence or dose (either from direct protons or from a mixed field – primarily neutrons, gammas, and electrons – beyond which the light transmission ceases. Specifically, after absorbed doses of 10 Grad (0.10 GGy) the transmittance for the three wavelengths (violet, blue and red) approached 10% of the unirradiated value for the 1 mm-diameter fibers and dropped below 10% for the 2 mm-diameter fibers. At higher absorbed doses, 28 Grad (0.28 GGy), the transmittance became essentially zero, regardless of the fiber diameter. While delineation of fiber absorbed dose between 10 Grad (10 GGy) and the peak of 28 Grad (0.28 GGy) achieved for the fibers located at the center of the proton beam, it was not possible to establish the exact dose at which their transmittance seizes.

The study has revealed big differences in transmission degradation linked to the fiber diameter where, the 2 mm diameter fibers experienced much greater transmittance loss than their 1 mm counterparts for similar dose. This was attributed to the orientation of the fibers relative to the impinging angle of irradiating protons, resulting in significantly greater lateral leakage of knock-on electrons and protons in the thinner (1 mm diameter) fibers thus leading to smaller damage. This convoluted effect of fiber diameter size and irradiating field will be explored in future studies.

Microscopic and optical examination of the fibers revealed extensive micro-structural damage features and irradiation-induced defects with defect density higher towards the upstream half of the 50 mm long fibers.

Future studies:

Silicon sensor irradiation and performance studies for the development of tracking and timing detectors for future hadron colliders, beyond the HL-LHC, will make use of proton and spallation neutron beams from the BNL 200 MeV Linac. More specifically, future hadron colliders, for example the CERN's Future Circular Collider (FCC-hh), will deliver larger instantaneous luminosities than those currently delivered by the LHC or those expected to be achieved by the HL-LHC. As a consequence, materials that are placed close to the interaction points, e.g. silicon tracking and timing detectors, will have to exhibit the necessary radiation resistance, i.e. up to integrated hadron fluences of the order of 10^{18} 1 MeV neutron equivalent/cm^2. The beam of 200 MeV proton will be used to replicate the effect of the charged hadrons (predominantly pions in the 0.1–1 GeV range) that dominate the damage in detectors placed closely to the interaction point. Displacement damage in silicon detectors will be studied by spallation neutrons generated from the same proton beam. The development of radiation-hard silicon detectors that can operate in such hard conditions as in future hadron colliders will need a long-term irradiation campaign with dedicated and nearly continuous testing, exploiting a positive feedback-loop of design, fabrication, irradiation and testing that can be carried out at BNL. Additionally, experiments accompanied with analytical studies are envisioned to address cross-fiber interaction and induced damage stemming from "leakage" emanating from thin fibers.

SiO_2 fiber irradiation, emulating fission and fusion reactor conditions and performance, will be addressed in the future by exploring the correlation of irradiating particle energy and induced damage through beam experiments (including mixed spectra) and Monte Carlo simulations. For fusion reactor diagnostics applications, these fibers will be required to function at fluences of $\sim 10^{22}$ n/cm^2 (14 MeV neutrons). The present study showed that the performance of the fibers for 28 Grad absorbed dose was similar to the performance (total loss of transmittance) with the one of 28 Grad dose from a mixed field of fast neutrons and γ-rays. The outlook obviously is not very encouraging from data to-date as deduced from the present study. The combined role of irradiating particle energy, irradiation temperature and the fiber diameter are parameters worths exploring further for potential applications in fusion and fission environments. The latter is prompted by the reported findings [10] where fibers performed well in terms of their radiation characteristics up to the fast neutron fluence of 1.06×10^{20} n/cm^2 (E > 1.0 MeV) during irradiation at elevated temperatures.

CRediT authorship contribution statement

N. Simos: Conceptualization, Formal analysis, Methodology, Resources, Supervision, Writing - original draft, Writing - review & editing. **G. Atoian:** Investigation, Validation, Writing - review & editing. **A. Bolotnikov:** Investigation, Validation, Writing - review & editing. **D. Sprouster:** Acquisition of data, Analysis and interpretation of data. **A. Tricoli:** Conceptualization, Methodology. **D. Medvedev:** Conceptualization, Data curation, Writing - original draft. **M. Palmer:** Resources, Supervision, Writing - review & editing. **D. Asner:** Mthodology, Software, Writing - review & editing. **N. Charitonidis:** Methodology, Software, Supervision, Writing - review & editing. **N. Mokhov:** Methodology, Software, Writing - review & editing. **Z. Kotsina:** Investigation, Methodology, Writing - review & editing.

Declaration of competing interest

The authors declare that they have no known competing financial interests or personal relationships that could have appeared to influence the work reported in this paper.

References

[1] N. Mokhov, MARS15 Studies of absorbed and residual doses in the TAN and LHCf and ZDC detectors, in: First TAN Integration Workshop, CERN, March 10, 2006, http://indico.cern.ch/conferenceDisplay.py?confId=920.

[2] A.J. Furgeri, et al., Radiation damage effects on CMS sensors quality assurance and irradiation tests, IEEE Trans. Nucl. Sci. 51 (6) (2004).

[3] B. Tsuchiya, et al., Correlation between radiation-induced defects, and optical properties of purefused silica-core optical fiber, under gamma-ray irradiation in air at 1273 K, J. Nucl. Mater. 417 (2011) 810–813.

[4] A. Morana, S. Girard, et al., Influence of neutron and gamma-ray irradiations on rad-hard optical fiber, Opt. Mater. Express 5 (4) 898. http://dx.doi.org/10.1364/OME.5.000898.

[5] E. Colby, et al., Gamma radiation studies on optical materials, IEEE Trans. Nucl. Sci. (2002).

[6] M. Jakši, et al., Comparison of proton microbeam and gamma irradiation for the radiation hardness testing of silicon PIN diodes, J. Instrum. 8 (2013) P09003.

[7] I.K. Abdukadyrova, IR Spectra of fused silica irradiated by fast neutrons, J. Appl. Spectrosc. 73 (4) (2006).

[8] W.D. Compton, et al., Radiation Effects in Fused Silica and α-Al_2O_3, U.S. Naval Research Laboratory, 1961, pp. 130–139.

[9] R.R. Gulamova, et al., Fused Silica in Ionizing Radiation Dosimetry, UDC 539.12.03.

[10] T. Shikama, et al., Optical properties in fibers during irradiation in a fission reactor, J. Nucl. Mater. 225 (1995) 324–327.

[11] T. Kakuta, et al., Behavior of optical fibers under heavy irradiation, Fusion Eng. Des. 41 (1998) 201–205.

[12] Alfeeli B. Pickrell, G. Garland, A. M. A. Wang, Behavior of random hole optical fibers under gamma ray irradiation and its potential use in radiation sensing applications, Sensors 7 (2007) 676–688.

[13] R.G. Ahrens, J.J. Jaques, M.J. Luvalle, D. Digivanni, R.S. Windeler, Radiation effects on optical fibers and amplifiers, in: Proceedings of Testing, Reliability, and Applications of Optoelectronic Devices, SPIE 4285 978 – 0 – 81943 – 963 – 5, SPIE, 2001, pp. 217–225.

[14] Fernando W. Gan, et al., Radiation-hard optical link for the ATLAS pixel detector, in: Presented at IEEE05, Puerto Rico, 2005.

[15] R.S. Fielder, R. Duncan, M. Palmer, Recent Advancements in Harsh Environment Fiber Optic Sensors: An Enabling Technology for Emerging Nuclear Power Applications, Luna Innovations, Inc., 2005.

[16] K.K. Gan, et al., Radiation-hard optical link for SLHC, J. Phys.: Conf. Ser. 110 (2008) http://dx.doi.org/10.1088/1742-6596/110/9/092011.

[17] H. Kimurai E. Takada Y. Hosono M. Nakazawa Takahashi. H. Hayami, New techniques to apply optical fiber image guide to nuclear facilities, J. Nucl. Sci. Technol. (ISSN: 0022-3131) 39 (6) (2002) 603–607.

[18] S. O'Keeffe, Fitzpatrick, et al., A review of optical fibre radiation dosimeters, Sensor Rev. (ISSN: 0260-2288) 28 (2) (2008) 136–142.

[19] R. Reichle, et al., Experimental developments towards an ITER thermography diagnostic, J. Nucl. Mater. (1466–1471) (2007) 363–365, http://dx.doi.org/10.1016/j.jnucmat.2007.01.207.

[20] S. Girard, et al., Overview of radiation induced point defects in silica-based optical fibers, Rev. Phys. 4 (2019) 100032.

[21] M. Moll, Radiation tolerant sensors for pixel detectors, in: PIXEL 2005 International Workshop, Sept. 2007, Bonn, Germany, 2007.

[22] L.F. Mausner, et al., The design and operation of the upgraded BLIP facility for radionuclide research and production, Int. J. Rad. Appl. Instrum. A 41 (4) (1990) 367–374.

[23] N.V. Mokhov, C.C. James, The MARS Code System User'S Guide, Version 15, 2016, Fermilab-FN-1058-APC (2017), https://mars.fnal.gov/;
N.V. Mokhov, et al., Prog. Nucl. Sci. Technol. 4 (2014) 496, http://dx.doi.org/10.15669/pnst.4.496.

[24] T.T. Böhlen, F. Cerutti, M.P.W. Chin, A. Fassò, A. Ferrari, P.G. Ortega, A. Mairani, P.R. Sala, G. Smirnov, V. Vlachoudis, The FLUKA code: Developments and challenges for high energy and medical applications, Nucl. Data Sheets 120 (2014) 211–214.

[25] A. Ferrari, P.R. Sala, A. Fasso, J. Ranft, FLUKA: A Multi-Particle Transport Code CERN-2005-10, INFN/TC_05/11, SLAC-R-773, 2005.